Viral satellites exploit phage proteins to escape degradation of the bacterial host chromosome

Amelia C. McKitterick[1], Stephanie G. Hays[1], Munirul Alam[2], and Kimberley D. Seed[1,3,*]

[1]Department of Plan and Microbial Biology, University of California, Berkeley, 271 Koshland Hall, Berkeley, CA 94720, USA

[2]icddr,b, formerly known as International Centre for Diarrhoeal Disease Research, Bangladesh, Dhaka, Bangladesh

[3]Chan Zuckerberg Biohub, San Francisco, CA 94158, USA

*Correspondance: kseed@berkeley.edu

Key words: phage, mobile genetic element, defense, replication, parasitism, satellite, helicase

Summary

Phage defense systems are often found on mobile genetic elements (MGEs), where they constitutively defend against invaders or are induced to respond to new assaults. Some MGEs, the phage satellites, exploit phages for their own transmission after induction, reducing phage production and protecting their hosts in the process. One such satellite in *Vibrio cholerae*, PLE, is triggered by the lytic phage ICP1 to excise from the chromosome, replicate, and transduce to neighboring cells, completely sabotaging phage production. Here, we found that ICP1 has evolved to possess one of two syntenic loci encoding an SF1B-type helicase, either of which PLE can exploit to directly drive PLE replication. Further, loss of PLE mobilization limits anti-phage activity due to phage-mediated degradation of the bacterial genome. Our work provides insight into the unique challenges imposed on the parasites of lytic phages and underscores the adaptions of these satellites to their ever-evolving target phage.

Introduction

Viruses and mobile genetic elements (MGEs) are associated with organisms from all branches of the tree of life (Koonin & Krupovic 2015). In order to successfully infect their hosts, viruses employ a variety of host-takeover programs that inhibit host activities while promoting viral processes. Bacteriophages, or phages, are viruses that infect bacterial hosts and have profound effects on bacterial fitness, as well as on human health and disease (Brüssow et al. 2004; Bondy-Denomy & Davidson 2014). Of interest, lytic phages, which infect and kill their bacterial hosts within a single round of infection, have recently come to light as having impactful roles in shaping the composition of bacterial populations, such as the human gut microbiome (Manrique et al. 2017), and as potential biocontrol agents for antibiotic resistant infections (Pires et al. 2016). Lytic phages are particularly insidious to their bacterial hosts—upon infection, phages like the lytic *Escherichia coli* phage T4 can express a variety of genes that mediate host-cell takeover programs. T4 expresses genes that shut down and redirect host transcriptional machinery to favor transcription of phage genes, as well as nucleases that degrade the host chromosome to inhibit host gene expression as well as free up nucelosides that are then incorporated into the rapidly replicating phage genome (Hinton et al. 2005; Warner et al. 1970; Hercules et al. 1971).

Paradoxically, phages also contribute to bacterial population diversity and complexity by facilitating horizontal gene transfer (HGT) (Brüssow et al. 2004; Koskella & Brockhurst 2014). In addition to the well characterized mechanisms by which phages can spread bacterial genetic material to neighboring cells, such as generalized and specialized transduction (Penadés et al. 2015), recent work has uncovered a means for large regions of the bacterial chromosome to be packaged into temperate phage virions in a process termed lateral transduction (Chen et al. 2018). Independent of packaging, phages can also facilitate the spread of bacterial plasmid DNA from lysed cells to neighbors, increasing the range of genetic material that can be shared within a population (Keen et al. 2017). In sharp contrast to these forms of “passive” phage-

mediated HGT, there are parasitic mobile genetic elements referred to as phage satellites, such as phage inducible chromosomal islands (PICIs), that have evolved to explicitly manipulate the phage replication and packaging programs for their own horizontal spread (Penadés & Christie 2015).

Typically, phage defense in bacteria is attributable to widely characterized systems, including restriction-modification and CRISPR-Cas systems that inhibit phage through targeted cleavage of the infecting phage genome, and toxin/antitoxin systems and abortive infection systems that function through killing of the infected host cell (Samson et al. 2013; Dy et al. 2014; Hille et al. 2018). However, phage parasites, which are being increasingly discovered (O'Hara et al. 2017; Martínez-Rubio et al. 2017; Fillol-Salom et al. 2018), can also provide robust phage defense for their bacterial hosts. One type of PICI, the well characterized *Staphlococcus aureus* pathogenicity islands (SaPIs), are induced by infection with a helper phage, compete with that helper over the bacterial host's replication machinery, and steal phage packaging proteins to selfishly package the SaPI genome for horizontal transfer. This parasitic interference negatively impacts the ability of the helper phage to complete its lifecycle, thus blocking plaque formation (Ubeda et al. 2009; Tormo-Más et al. 2010; Ram et al. 2012). Despite diverse mechanisms, phage defense systems must overcome phage-mediated host takeover and go on to prevent rampant phage propagation through the bacterial community. Genomic analyses to localize anti-phage mechanisms in bacterial genomes have revealed that they tend to cluster together on what are referred to as defense islands (DIs) (Makarova et al. 2011). Analysis of DIs has even led to the discovery of new phage defense systems solely due to the prevalent clustering of these defense systems on MGEs (Doron et al. 2018). While hypothesized to have roles in HGT, the prevalence of phage defense systems on genomic islands has yet to be explained. Likewise, it remains to be seen the extent to which such DIs have evolved to parasitize phages for their own dissemination.

Vibrio cholerae, the etiological agent of the diarrheal disease cholera, is constantly under assault by phages both in aquatic environments as well as in human hosts (Faruque et al. 2005; Seed et al. 2011; Seed et al. 2014). The dominant phage that preys on epidemic *V. cholerae* is ICP1, a lytic myovirus that is consistently isolated from cholera patient stool samples in regions where cholera is endemic, such as Dhaka, Bangladesh (Seed et al. 2011; Angermeyer et al. 2018; McKitterick et al. 2019). In response to the consistent attack by ICP1, *V. cholerae* has acquired the phage-inducible chromosomal island-like element (PLE), a highly specific phage satellite that blocks plaque formation by ICP1 while exploiting phage resources to further its lifecycle (O'Hara et al. 2017). PLE excises from the host chromosome during ICP1 infection, replicates to high copy, and is specifically transduced to neighboring cells; concurrently, PLE replication within the host cell negatively impacts the ability of ICP1 to replicate its genome, contributing to the inhibition of ICP1 production (Barth et al. 2019). PLE encodes a large serine recombinase, Int, that catalyzes the PLE excision and circularization reaction by physically interacting with ICP1-encoded PexA, a small protein of unknown function that is specific to ICP1 and is hijacked by PLE to act as a recombination directionality factor (McKitterick & Seed 2018). Once excised, PLE begins to replicate and then is thought to steal structural proteins from ICP1 to facilitate its own transmission. Once packaged, PLE triggers accelerated lysis of the infected culture allowing for release of PLE transducing particles from the infected cells, ultimately killing the infected *V. cholerae* host but protecting the population as no infectious ICP1 progeny are produced (O'Hara et al. 2017). Five PLEs have been identified in epidemic *V. cholerae* isolates and all block plaque formation by ICP1. In addition to inhibiting ICP1, PLEs are also characterized by conserved genomic architecture and the aforementioned PLE lifecycle during ICP1 infection (O'Hara et al. 2017).

Recent work has uncovered a PLE-encoded factor that is necessary for PLE replication: the replication initiation factor, *repA* (Barth et al. 2019). Expression of *repA* is induced by ICP1 infection (unpublished), facilitating origin binding and recruitment of replisome proteins that have

yet to be identified. In the absence of ICP1 infection, however, RepA is not sufficient to drive PLE replication (Barth et al. 2019), further, PLE is not predicted to encode replication machinery, suggesting that other phage-encoded gene products are required for PLE amplification. As all PLEs replicate following ICP1 infection (O'Hara et al. 2017), it stands to reason that the PLE has evolved to exploit conserved components of ICP1's replication machinery. Similar to PLE excision (O'Hara et al. 2017), PLE replication is essential for horizontal transmission of PLE transducing units, thus further underscoring the role of ICP1 in driving PLE HGT; however, the relatively low rate of transduction suggests that robust PLE replication may have other roles in the PLE conflict with ICP1 (Barth et al. 2019).

In order to exploit ICP1, PLE must escape from ICP1-mediated host takeover during infection. While the precise mechanisms that ICP1 uses to overcome *V. cholerae* have not been characterized, ICP1 is able to rapidly begin replicating its genome following infection (Barth et al. 2019) and produces about 100 virions within 20 minutes of infection (O'Hara et al. 2017). Here, we identify ICP1 *ΔpexA* mutants that escape PLE by acquiring mutations in the ICP1-encoded SF1B accessory helicase that we have named *helA*. We show that while this helicase is not necessary for ICP1 replication, it is essential for PLE to hijack to drive its own replication during ICP1 infection. We show that the excision- and replication-deficient PLE is susceptible to ICP1-mediated host takeover, whereby PLE is degraded while it remains integrated in the *V. cholerae* chromosome. Analysis of natural isolates of ICP1 from cholera patient stool samples in the megacity of Dhaka compared to a rural site in Bangladesh revealed an alternative SF1B helicase allele in phages shed from the rural site. Functional comparisons between the two alleles revealed that both alleles, though unrelated, can be hijacked by all PLEs to facilitate PLE replication. Though neither helicase is essential for ICP1, ICP1 faces impaired fitness in the absence of either accessory helicase, explaining their prevalence in ICP1 and other *Vibrio* phages. PLE's capacity to use a variety of phage-encoded helicases to drive PLE replication underscores the critical role that replication plays in the PLE lifecycle to avoid phage-mediated

host takeover and to facilitate continued gene expression. The common trend of phage defense islands clustering on MGEs suggests that mobilization of these phage defense islands, such as PLE, is a common mechanism to escape phage mediated host takeover.

Results

ICP1 is able to escape excision deficient PLE by acquiring mutations in the predicted helicase *helA*

Previous work has demonstrated the role for phage-encoded *pexA* in directing PLE 1 excision during infection with an ICP1 isolate from 2006, referred to as ICP1^{A} (McKitterick & Seed 2018) (Figure 1A). PLE 1 mediated inhibition of ICP1 does not require PLE 1 excision, so ICP1 *ΔpexA* is still blocked by PLE 1 (Figure 1B); however, ICP1^{A} *ΔpexA* is able to form rare plaques on *V. cholerae* harboring PLE 1 at a frequency of about 1 per 10^{6} phage (Figures 1A and 1C). Due to the low efficiency of plaquing, we consider these phage to be “escape phage” that have acquired a mutation in the genome allowing them to overcome PLE 1. To identify the phage gene(s) that harbor mutations enabling escape, we collected and purified three escape phage and performed whole genome sequencing. Analysis of these genomes revealed that all escape phage had acquired mutations in ICP1^{A} *gp147*, a predicted SF1B-type helicase which we have since named *helicase A* (*helA*) (Table S1).

SF1B-type helicases are found broadly across all domains of life and include the well-studied *pif1* and *recD* (Saikrishnan et al. 2009). In eukaryotes such as *Saccharomyces cerevisiae*, *pif1* has been implicated in telomere maintenance, Okazaki fragment processing, and resolution of G-quadruplex motifs (Byrd & Raney 2017), while *recD* is a core component of the *E. coli* RecBCD complex involved in DNA processing and repair (Singleton et al. 2004). Another prototypical SF1B-type helicase is *dda,* encoded by phage T4, which is a non-essential accessory helicase implicated in origin melting, translocating proteins off DNA, and a wide

158 variety of other functions *in vitro*, although its exact role *in vivo* is unknown (He et al. 2012; Byrd
159 & Raney 2006; Brister 2008).

160 To validate the role of *helA* in ICP1^{A} escape from PLE 1, we constructed a *helA* deletion
161 in a wild-type ICP1^{A} background and probed the mutant phage for the ability to overcome PLE
162 1. ICP1^{A}-encoded *helA* is not necessary for plaque formation on PLE (-) *V. cholerae*, and ICP1^{A}
163 *ΔhelA* is still blocked by PLE 1, indicating that *helA* is not necessary for PLE 1 induction (Figure
164 1B). Similar to ICP1^{A} *ΔpexA*, the absence of *helA* gives ICP1^{A} an advantage on PLE (+) *V.*
165 *cholerae*, allowing for rare plaques to form; however, ICP1^{A} *ΔhelA* forms plaques at a frequency
166 two orders of magnitude higher than ICP1^{A} *ΔpexA* on PLE 1 (Figure 1C). Conversely, the
167 double mutant ICP1^{A} *ΔpexA ΔhelA* is able to form small plaques on PLE 1 at a relatively high
168 efficiency (Figures 1B and 1C). ICP1^{A} *ΔpexA ΔhelA* plaques that form on PLE (+) *V. cholerae*
169 were picked and the plaquing efficiency was re-tested to determine if those phage were
170 subsequently able to escape PLE 1 at a higher rate (Figure S1). As these progeny phage re-
171 plaqued at the same efficiency as ICP1^{A} *ΔpexA ΔhelA*, we conclude that they are not genetic
172 escape phage but instead are able to overcome some aspects of PLE 1 activity through the loss
173 of both ICP1^{A}-encoded *pexA* and *helA*.

174 We next wanted to characterize the role of *helA* for ICP1^{A} function. HelA is detectable in
175 infected cells via Western blot within eight minutes of ICP1^{A} infection (Figure 1D), which is
176 consistent with the onset of ICP1^{A} replication initiation (Barth et al. 2019), suggesting that *helA*
177 may have a role in ICP1^{A} replication. As PLE 1 diminishes the level of ICP1^{A} replication (O'Hara
178 et al. 2017; Barth et al. 2019), we hypothesized that PLE 1 hijacks HelA during infection as a
179 mechanism to interfere with ICP1^{A} replication. To test this hypothesis, we evaluated ICP1^{A}
180 *ΔhelA* replication in the presence and absence of PLE 1 by qPCR. In contrast to plaque
181 formation, which requires multiple rounds of phage infection and replication to visualize a zone
182 of killing, qPCR allows for quantification of phage DNA replication in a single round of infection.
183 Consistent with the ability to form a plaque on PLE (-) *V. cholerae*, there are no deficiencies in

ICP1^{A} *ΔhelA* replication relative to a wild-type phage over the course of the 20 minute infection cycle (Figure 1E), indicating that *helA* is not essential for ICP1^{A} replication. Conversely, infection of a PLE (+) *V. cholerae* host with ICP1^{A} *ΔhelA* rescues ICP1 replication to the level that is observed in a PLE (-) host (Figure 1E), suggesting that, while not necessary for ICP1^{A}, *helA* is exploited by PLE 1 to interfere with ICP1 during infection. However, because ICP1^{A} *ΔhelA* is not deficient for replication in the absence PLE 1, the ICP1^{A} replication defect in the presence of PLE 1 is not likely directly due to PLE 1-mediated hijacking of HelA activity.

ICP1-encoded *helA* is necessary for PLE replication

ICP1 and PLE 1 replication appear to be inversely related, wherein ICP1 copy number is restored when PLE 1 replication is abolished via deletion of either the PLE 1 origin of replication or *repA* (Barth et al. 2019). Therefore, the observed restoration in ICP1^{A} *ΔhelA* copy number during infection of a PLE (+) host implicates phage-encoded HelA in promoting PLE 1 replication. To test the role of *helA* in PLE replication, we infected PLE (+) *V. cholerae* with ICP1^{A} *ΔhelA* and monitored the change in PLE 1 copy over the course of infection. While PLE 1 is able to replicate to high copy when infected with a wild-type phage, strikingly, PLE 1 is unable to replicate in the absence of *helA* (Figure 2A). This phenotype can be complemented by ectopic expression of *helA* during ICP1^{A} infection, demonstrating that *helA* is necessary for PLE 1 replication.

SF1B-type helicases are implicated in activities ranging from replication and genome maintenance to transcriptional regulation (Byrd & Raney 2017). Additionally, the *S. aureus* phage parasites, SaPIs, make use of dUTPases as anti-repressors to initiate the transcriptional program of the island, suggesting that these genomic islands can evolve to respond to phage-encoded proteins independent of their biological function for the phage (Tormo-Más et al. 2010; Bowring et al. 2017). As such, we next wanted to determine if *helA* has a direct role in PLE 1 replication or if it is necessary to transcriptionally activate the island to allow for production of

PLE 1-encoded proteins, such as *repA*, that are essential for PLE 1 replication. To test the involvement of *helA* in PLE 1 replication, we made use of a minimal PLE replication system referred to as the "midiPLE" (Barth et al. 2019). The midiPLE contains only the endogenous PLE 1 integrase as well as the PLE 1 origin of replication, integrated in the same chromosomal location as PLE 1 in the *V. cholerae* chromosome. This construct is competent to excise from the chromosome following *pexA* expression during ICP1^{A} infection, but is unable to replicate without ectopic expression of the PLE 1-encoded replication initiator, *repA*. When *repA* is provided *in trans*, midiPLE replicates during ICP1^{A} infection (Figure 2B). In comparison to infection with wild-type phage, midiPLE fails to replicate during infection with ICP1^{A} *ΔhelA*. This phenotype can be complemented by expressing *helA in trans*, showing that *helA* is necessary for PLE 1 replication independent of other PLE 1-encoded genes and supporting the conclusion that HelA is directly involved in PLE 1 replication. Interestingly, *helA* is not sufficient to stimulate PLE 1 replication in the absence of ICP1^{A} infection (Figure 2B), indicating that other phage, or possibly *V. cholerae*, components are additionally required to facilitate PLE 1 replication.

PLE replication contributes to anti-phage gene dosage

In the course of replication sampling during ICP1^{A} infection, we observed a defect in PLE 1-mediated accelerated lysis that correlates with a loss in PLE 1 replication. A culture of PLE (+) *V. cholerae* infected with ICP1 typically lyses 20 minutes after infection, while an infected PLE (-) culture takes upwards of 90 minutes to lyse (O'Hara et al. 2017). However, we observed that cultures infected with ICP1^{A} *ΔhelA* consistently had delays in lysis, suggesting impaired PLE 1 activity, and ectopic expression of *helA* led to intermediate lysis phenotypes (Figure S2A). Though the basis for PLE 1-mediated accelerated lysis is not yet known, we reasoned that robust PLE 1 replication enhances expression of PLE 1-encoded genes merely through increasing the template copy number. To test this hypothesis, we created a nanoluciferase transcriptional reporter cloned downstream of PLE 1 *orf2* (P_{orf2}*nanoluc*, Figure

S2B) to quantify defects in PLE 1 transcription when PLE 1 is unable to replicate. Relative to infection with wild-type ICP1^{A}, P$_{orf2}$*nanoluc* produced 0.16 times as much luminescence during infection with ICP1^{A} *ΔhelA* (Figure 2C). When PLE 1 replication was restored through ectopic expression of *helA*, the reporter activity resulting from infection with ICP1 *ΔhelA* was restored to wild-type levels, demonstrating that PLE 1 copy number contributes to the global level of PLE 1 transcription. As such, inhibition of PLE 1 replication leads to phenotypes such as delayed lysis during ICP1^{A} infection and potentially contributes to the ability of ICP1^{A} *ΔhelA* to escape PLE 1.

ICP1 overcomes replication and excision deficient PLE through degradation of the *V. cholerae* chromosome

As ICP1-encoded *pexA* is necessary for PLE 1 excision (McKitterick & Seed 2018) and *helA* is necessary for PLE 1 replication during ICP1 infection (Figure 2A), we next wanted to understand how ICP1^{A} *ΔpexA ΔhelA* is able to overcome PLE 1 (Figure 1B). Even when PLE 1 is challenged by ICP1^{A} *ΔhelA* and is unable to replicate leading to transcriptional deficiencies, PLE 1 is still able to excise from the *V. cholerae* chromosome and is more inhibitory than when it is maintained in the chromosome, leading us to speculate that the position of PLE 1 in the cell, either intra- or extrachromosomal, is important for its activity. Phages are known to encode nucleases that attack the bacterial chromosome, freeing up nucleosides that can then be incorporated into newly synthesized phage genomes (Warner et al. 1970). Additionally, deep sequencing of the total DNA in ICP1 infected *V. cholerae* cells shows that the proportion of reads mapping to the *V. cholerae* chromosomes decreases over the course of infection (Barth et al. 2019). This observation led us to hypothesize that nucleolytic activity encoded by ICP1^{A}, deployed to degrade the *V. cholerae* chromosome during infection, is able to degrade PLE 1 when PLE 1 is stuck in the chromosome unable to replicate, allowing for ICP1^{A} to form some small plaques on PLE (+) *V. cholerae*. To test this hypothesis, we made use of a minimal PLE excision system, the miniPLE, that has the PLE 1-encoded integrase but lacks an origin of

replication (Figure 3A). Thus during infection, the miniPLE excises from the host chromosome and circularizes, but does not replicate (McKitterick & Seed 2018). To simulate an excision-deficient miniPLE, we created miniPLE$_{CD}$, which possesses a point mutation in the catalytic serine residue in the miniPLE-encoded integrase, making the integrase catalytically dead and rendering the construct unable to excise from the chromosome (Figure 3B).

Total DNA from ICP1^{A} miniPLE and miniPLE$_{CD}$ infected cells was digested, run on an agarose gel, and the stability of the miniPLE was observed via Southern blot (Figure 3C). During the course of ICP1^{A} infection, the miniPLE successfully excises from the *V. cholerae* chromosome and is maintained as an episome. Conversely, the amount of miniPLE$_{CD}$, which is unable to excise from the chromosome, decreases by 20 minutes following ICP1^{A} infection (Figure 3C, bottom), relative to the amount of total DNA prepped from the cells (Figure 3C, top), suggesting that the copy number of miniPLE$_{CD}$ decreases as a result of ICP1^{A} infection. Quantification of miniPLE via qPCR further demonstrates that the excision-competent miniPLE is maintained as a stable episome with no change in copy number during ICP1^{A} infection (Figure 3D). In comparison, the miniPLE$_{CD}$ that is unable to escape the *V. cholerae* host chromosome decreased in copy number during infection with ICP1^{A}, indicating that it is susceptible to ICP1^{A}-mediated chromosomal degradation. Thus, not only is PLE mobilization important for HGT (O'Hara et al. 2017; Barth et al. 2019), but it is also essential for PLE escape from ICP1 takeover of the *V. cholerae* host.

Diverse SF1B helicases are maintained in ICP1 and contribute to ICP1 fitness

Due to the importance of PLE replication in PLE gene dosage and avoiding ICP1-mediated host takeover, we next hypothesized that ICP1 would evolve to abolish PLE replication by accumulating mutations in the *helA* allele, indicative of co-evolution between the two entities. To identify signatures of co-evolution, we examined HelA from sequenced isolates of ICP1 that had been recovered from epidemic sampling in Dhaka, Bangladesh. HelA from

ICP1 isolated from epidemic sampling from 2001 to 2017 is over 99% identical at the amino acid level indicating that there is either little pressure for HelA to evolve over time, or that HelA mutations cannot be tolerated in nature (Table S6). Though there is no change in the ability of ICP1 to replicate in a single round of infection in the absence of *helA* (Figure 1E), ICP1^{A} *ΔhelA* forms plaques that are on average 0.75 times smaller than wild-type phage plaques (Figure 4A). This size defect indicates that mutant phage are less fit in the absence of *helA* and supports the notion that functional *helA* must be maintained by ICP1 in nature.

Despite having a high degree of conservation, *helA* is not considered part of the core ICP1 genome (Angermeyer et al. 2018): two phage isolates recovered from cholera patient stool samples from Dhaka in 2006 do not encode *helA*, but instead have an alternative SF1B-type helicase in the same locus, which we call *helicase B* (*helB*) (Figure 4B). HelB is 24% identical to HelA, with a conserved P-loop ATPase domain, but HelB has an extended C-terminus that contains a domain of unknown function, DUF2493 (Figure S3A). In addition to having low sequence identity, *helA* and *helB* are flanked by different, unrelated genes each encoding products with no predicted structure or function (Figure 4B), suggesting that while ICP1 is unable to lose *helA* in nature in an attempt to avoid hijacking by PLE for replication, ICP1 may swap *helA* for a distinct accessory helicase.

We then performed a BLASTP search of the National Center for Biotechnology Information's nonredundant protein sequence database to identify the origin of *helA* and *helB*. Homologs of HelA are commonly found in phages of marine bacteria, and, particularly, in a group of related myoviruses that infect non-cholera *Vibrios* (Figure S3B). Of note, two of the *Vibrio* phages were also predicted to encode a homolog of one of the proteins flanking HelA in ICP1^{A}, indicating that the *helA* locus could have been shared with a common ancestor of these phages. Conversely, HelB is more divergent, with the only identifiable homolog found in a *Pseudoalteromonas* phage that is also predicted to have the same DUF2493 C-terminus. These HelB proteins cluster on a more distant branch than the HelA homologs (Figure S3B),

supporting the hypothesis that *helB* was horizontally acquired by ICP1. Altogether, SF1B helicases are readily found in marine phages, and ICP1 encoding *helA* are the dominant ICP1 shed by cholera patients in Dhaka between 2001-2017.

Most epidemic sampling of ICP1 from cholera patients has been done in the urban cholera endemic site in Dhaka; however, we recently began sampling cholera patients at a rural and estuarine site in Mathbaria, Bangladesh. In contrast to what was observed in ICP1 isolates from Dhaka in the 2017 epidemic period, all the ICP1 isolates recovered from cholera patients in Mathbaria encoded the *helB* allele (Figure 4C). One representative isolate from Mathbaria from 2017, referred to here as ICP1^{B}, is over 99.8% identical to ICP1^{A} across 90% of the genome, with 205 of 227 ICP1^{B} predicted open reading frames being shared with ICP1^{A}. The resurgence and dominance of *helB* in the Mathbaria epidemic sampling suggests that there could be a selective advantage for ICP1 encoding *helB* rather than *helA* in this region.

As ICP1^{B} is not isogenic to ICP1^{A}, we first wanted to characterize the role of *helB* in ICP1^{B} fitness. Similar to HelA, HelB is detectable by Western blot within 8 minutes of infection (Figure 5A), again coinciding with ICP1 replication (Barth et al. 2019). Also similar to *helA*, *helB* is not essential for ICP1^{B}, and ICP1^{B} *ΔhelB* is able to form plaques in the absence and presence of PLE 1 (Figure 5B). Interestingly, ICP1^{B} *ΔhelB* forms plaques on PLE (+) *V. cholerae* with a higher efficiency than ICP1^{A} *ΔhelA*, suggesting that ICP1^{B} has evolved other ways to limit PLE-mediated anti-phage activity.

We next wanted to see if ICP1^{B} replication was impacted by the *helB* deletion. In contrast to *ΔhelA* in ICP1^{A}, ICP1^{B} *ΔhelB* is significantly impaired for replication during the course of infection compared to wild-type ICP1^{B} (Figure 5C), indicating that although *helB* is not necessary for ICP1^{B} replication, it does have a more central role in phage fitness. Consistent with the observation that PLE 1 decreases the ability of ICP1^{A} to replicate (Figure 1E), replication of ICP1^{B}, too, is impacted negatively by PLE 1; however, ICP1^{B} *ΔhelB* does not restore the ability of ICP1^{B} to replicate in the presence of PLE 1 (Figure 5C), demonstrating a

more severe fitness effect associated with losing the accessory helicase on ICP1^{B} than on ICP1^{A} independent of the presence of PLE 1.

To confirm the role of *helB* in diminished ICP1^{B} fitness, we next ectopically expressed *helB* to complement the mutant phage. However, we could not complement the replication defect for ICP1^{B} *ΔhelB* by ectopic expression of *helB*, suggesting that the observed decrease in ICP1 fitness may not be due to direct loss of the *helB* gene product (Figure 5D)**.** To minimize potential polar effects of Δ*helB*, a targeted mutation was made to remove 25 amino acids encompassing the helicase domain (HD) that contains the Walker A motif necessary for ATP hydrolysis (Blair et al. 2009). While ICP1^{B} *helB ΔHD* had increased phage replication relative to the clean *helB* deletion, there was still a defect in replication that could not be complemented (Figure 5D), suggesting that ectoptic expression may not be able to achieve the appropriate timing or dosage of *helB* expression, or that the fitness cost is not a result of loss of HelB *per se*. Due to the complex nature of phage genomes and tight regulation of phage gene expression, disruption of even the HD domain of *helB* could have detrimental effects on uncharacterized *in cis* sites that could contribute to poor fitness. The fitness defect associated with mutant *helB* was also observed as a decrease in plaque size, with both ICP1^{B} *ΔhelB* and ICP1^{B} *helB ΔHD* forming plaques that are, on average, less than 0.66 times the size of ICP1^{B} (Figure 5E). Altogether, ICP1^{B} is less fit in the absence of *helB*, consistent with the observation that all natural ICP1 isolates encode one of two SF1B-type helicases, either *helA* or *helB*.

PLE exploits phage-encoded distinct SF1B-type helicases to drive replication during ICP1 infection

Given that PLE 1 replication requires *helA* (Figure 2A), and ICP1 with *helB* are dominant in Mathbaria*,* we were tempted by the possibility that phage with *helB* could be selected for as a mechanism to impede PLE 1 replication during infection. Hence, we next assessed if *helB* could also support PLE 1 replication. Consistent with the inverse relationship between ICP1 and PLE

1 replication, PLE 1 still replicated when infected with ICP1^{B}, and as with *ΔhelA*, PLE 1 replication was not observed in the absence *helB* (Figure 6A), indicating that *helB* is also necessary for PLE 1 replication despite HelB having less than shared 25% shared amino acid identity with HelA (Figure S3A). Further, ectopic expression of *helB* complemented the defect in PLE 1 replication observed during infection with ICP1^{B} *ΔhelB,* and ectopic expression of *helA* was likewise sufficient to restore PLE 1 replication during infection with ICP1^{B} *ΔhelB* (Figure 6A). These data demonstrate that PLE 1 is able to harness either ICP1-encoded accessory helicase independent of the ICP1 isolate that is infecting the host. Additionally, the shared ability of these non-isogenic ICP1 isolates to drive PLE 1 replication implicates functionally conserved gene products in ICP1 isolates, in addition to *helA* and *helB*, that are required for PLE 1 replication.

Similar to *helA,* we next used ICP1^{B} *ΔhelB* to probe for midiPLE replication following ectopic expression of *repA*. As expected, midiPLE replicated when infected with ICP1^{B} but failed to replicate in the absence of *helB*, indicating that *helB* is also directly involved in PLE 1 replication (Figure 6B). Like *helA*, *helB* is also not sufficient to stimulate PLE 1 replication in the absence of ICP1^{B}, showing that PLE 1 is still dependent on additional replication machinery from ICP1^{B}. We additionally confirmed that the ability of HelB to hydrolyze ATP is required for HelB to facilitate PLE 1 replication by testing the ICP1^{B} *helB ΔHD* variant, and, as anticipated, the helicase activity of *helB* is necessary for PLE 1 replication (Figure 6C).

The first ICP1 isolate identified with the *helB* allele was from Dhaka in 2006 when PLE 2 *V. cholerae* were being shed by cholera patients (O'Hara et al. 2017; McKitterick et al. 2019), leading us to evaluate if the two helicase alleles have different capacities to facilitate replication of different PLEs during infection with ICP1. To test this hypothesis, we first infected isogenic *V. cholerae* harboring each of the five characterized PLEs with ICP1^{A} and observed that all PLEs replicated equally well (Figure S4). Next, we determined that *helA* is necessary for replication of all five PLEs during ICP1^{A} infection and that replication can be complemented with ectopic

392 expression of *helA* (Figure 6D). To evaluate if each PLE can additionally use *helB* to support
393 replication, we also complemented ICP1^{A} *ΔhelA* with ectopic expression of *helB* and found that
394 in fact all five PLEs can use either one of the two ICP1-encoded accessory helicases for
395 replication.

396 As current data supports the model that PLE responds specifically to ICP1 infection
397 (O'Hara et al. 2017; McKitterick & Seed 2018), we next wanted to determine if PLE's capacity to
398 exploit either *helA* or *helB* to drive PLE replication is specific to ICP1-encoded proteins or in
399 general to SF1B-type helicases. To address the specificity of the interaction, we ectopically
400 expressed the SF1B-type helicase *dda from E. coli* phage T4 during infection with either ICP1^{A}
401 *ΔhelA* or ICP1^{B} *ΔhelB*. T4 Dda is only 16% identical to either HelA or HelB and does not group
402 with the marine phage SF1B-type helicases (Figure S3B). Although PLE 1 cannot replicate
403 while infected with either of these *Δhel* phage alone (Figures 6A and 6D), expression of *dda*
404 was sufficient to support PLE 1 replication in the absence of ICP1-encoded accessory helicases
405 (Figure 6E). Despite the apparent specificity between PLE and ICP1, the ability of PLE to exploit
406 a variety of phage-encoded accessory helicases reveals flexibility in at least one requirement for
407 PLE replication, and suggests that swapping of helicase alleles by ICP1 isolates is not a
408 beneficial strategy to mitigate PLE parasitism.
409

410 **Discussion**

411 In order to defend against viral infection, host resistance mechanisms must have ways
412 by which they prevent or bypass virus mediated host takeover. Eukaryotic DNA and RNA
413 viruses broadly use virally encoded ribonucleases to globally degrade host transcripts in the
414 infected cell, which sabotage their hosts through modulation of transcript and protein levels.
415 This decrease in transcript abundance leads to a downregulation of innate immune responses,
416 processes which are detrimental to the host but are ultimately reversable (Crow et al. 2016;
417 Rivas et al. 2016). Conversely, degradation of the host chromosome is a host takeover process

that is unique to phages. Host chromosome degradation has a twofold benefit for the predatory phages: it cleaves and releases nucleosides that can be incorporated into the rapidly replicating phage genome, and it can also destroy the template needed for expression of anti-phage genes encoded by the bacterial host. With the imminent shutdown of the host upon phage infection, it is not surprising to find that many bacterial defense systems, such as restriction-modification and some CRISPR-Cas systems, are expressed constitutively. By balancing the ability to discern between self and non-self, these systems are safely deployed in the absence of infection. Conversely, more self-destructive defense mechanisms, such as toxin/antitoxin systems and abortive infection systems cannot be constitutively active due to lethal outcomes and must be induced upon infection. Thus, for an inducible defense system like PLE, and perhaps many phage parasites, mobilization to evade host shutdown is critical. When PLE is unable to replicate or excise from the chromosome, it no longer fully blocks plaque formation by ICP1 and is susceptible to ICP1-mediated degradation of *V. cholerae's* chromosomes.

As a defense island and phage parasite of ICP1, the *V. cholerae* PLE has become highly evolved to make use of phage-encoded gene products to drive its anti-phage program (McKitterick & Seed 2018). Here, we characterize a new ICP1-PLE interaction: PLE hijacks a non-essential ICP1-encoded SF1B-type helicase to drive PLE replication during infection, making PLE the first characterized phage satellite that makes use of replication machinery encoded by its helper phage. In comparison, the well-studied SaPIs make use of their bacterial host's replication machinery and are able to autonomously replicate in the absence of helper phage (Úbeda et al. 2008). PLE's unique requirement for the phage-encoded helicase also underscores the differences between the helper phages that induce these chromosomal islands, with PLE being induced by a lytic phage that encodes its own replication machinery and SaPIs being induced by an activated temperate phage that also exploits its host-encoded replication machinery (Úbeda et al. 2008). The fact that *helA* expression alone is not sufficient to drive midiPLE replication in the absence of ICP1 infection implicates other ICP1-encoded replication

444 proteins in facilitating PLE replication. Aside from the SF1B-type helicases, the potential role for
445 ICP1's replication machinery in PLE replication remains to be elucidated. As T4 *dda* has been
446 observed to have a role in T4 origin initiation during origin-dependent replication (Brister 2008),
447 we speculate that *helA* has a similar role in facilitating origin firing in PLE by interacting with a
448 conserved part of the PLE machinery and recruiting a conserved ICP1 replication protein. ICP1
449 is predicted to encode a DNA polymerase and primase/helicase reminiscent of machinery that
450 drives the *E. coli* phage T7 replisome (Barth et al. 2019). Further work remains to identify what
451 roles, if any, these replisome proteins have in PLE mobilization.

452 Despite not being essential, all ICP1 isolates encode an accessory SF1B-type helicase,
453 as do several marine phages (Figure S3B) (Kauffman et al. 2018). Of note, one of these marine
454 *Vibrio* phages is also predicted to encode a complete Type 1-F CRISPR-Cas system, which is
455 of the same type that is encoded by some isolates of ICP1 to target and overcome PLE activity
456 (Seed et al. 2013; McKitterick et al. 2019), suggesting that ICP1 could be exchanging genetic
457 material with or could be related to these marine phages infecting non-cholera *Vibrios*. The
458 fitness costs associated with losing the accessory SF1B-type helicase, as measured by plaque
459 size, implicate both *helA* and *helB* in maintaining optimal phage fitness, though the precise role
460 for these accessory helicases in the phage lifecycle remains to be determined. The ease with
461 which PLE is able to make use of ectopically expressed *helB* compared to the inability of
462 ectopically expressed *helB* to complement the ICP1^{B} *ΔhelB* replication deficiency suggests that
463 these helicases play a specialized role in the phage lifecycle that is more complex than for PLE.

464 Due to the variability between ICP1 isolates, we see that PLE has evolved to make use
465 of not just two unrelated ICP1-encoded helicases, but also of T4 *dda*, the prototypical but
466 unrelated SF1B helicase. The ability of PLE to replicate using several dissimilar helicases
467 implicates strong evolutionary pressures for maintenance of PLE replication in response to ICP1
468 evolution. While *helA* is only one of the seemingly wide variety of ICP1 inputs that contribute to
469 PLE activity, SaPIs have similarly evolved to overcome variability in helper phage induction

cues (Bowring et al. 2017). The apparent promiscuity of the SaPI master repressor allows for recognition of structurally dissimilar but functionally conserved phage proteins to ensure SaPI excision, replication and spread, despite their helper phage's attempts to avoid SaPI induction. It is also imperative for PLE to be able to make use of either one of the ICP1-encoded helicases to continue PLE propagation through epidemic *V. cholerae* populations, thus selecting for PLE genes that are able to make use of dissimilar helicases despite the capacity of ICP1 to swap one helicase for another.

The striking spatial separation between the ICP1^{A} and ICP1^{B} populations that were shed by cholera patients in Bangladesh during the same epidemic period suggests that slight variations in the phage strain, such as the difference between *helA* and *helB*, can have large differences in the makeup of phage populations. Indeed, the ability of ICP1^{B} *ΔhelB* to form plaques in the presence of PLE (Figure 5B) suggests that ICP1^{B} should dominate in the presence of PLE (+) *V. cholerae*; however, the greater fitness cost for ICP1^{B} in the absence of *helB*, as evidenced by the diminished ability of ICP1^{B} *ΔhelB* to replicate, suggests that the loss of *helB* in the presence of PLE (+) *V. cholerae* is ultimately detrimental to the phage population.

The necessity of excision and replication of PLE during ICP1 infection highlights a crucial role for mobilization of inducible phage defense systems during phage infection. In order for inducible defenses to functionally protect a host cell from phage infection, they must be able to overcome the infecting phage's destruction of the host chromosome. Elements independent of the host chromosome, such as plasmids, seem to be somewhat protected from degradation by lytic phages (Keen et al. 2017). It thus stands to reason that the observed high prevalence of phage defense systems encoded on genomic islands (Makarova et al. 2011) may be in part due to the ability of genomic islands to mobilize during infection and escape phage-mediated host takeover, with the potential of horizontal transfer or the ability to escape from a dying host as an added benefit. Through experimental and *in silico* validation, more phage defense islands have been identified and characterized, albeit often in a context independent from infection by a

native phage. Given the propensity of some phages to degrade their host chromosome during infection and the need for protective MGEs to escape host takeover, it will be interesting to further explore if other inducible defense islands mobilize in response to phage infection and are in fact unrecognized phage satellites.

ACKNOWLEDGMENTS

This research was funded by the National Institute of Allergy and Infectious Diseases grant number R01AI127652 (K.D.S.). A.C.M. received support from the Kathleen L. Miller Fellowship from the Henry Wheeler Center for Emerging and Neglected Diseases. K.D.S. is a Chan Zuckerberg Biohub Investigator. The authors are especially thankful to icddr,b hospital and laboratory staff for their support, in particular Shirajum Monira, Fatema-tuz Johura, Marzia Sultana, Kazi Zillur Rahman, and Monika Sultana. M.A. of icddr,b, thanks the governments of Bangladesh, Canada, Sweden, and United Kingdom for providing core/unrestricted support. We also wish to thank members of the Seed Lab for helpful discussions, and Angus Angermeyer, specifically, for help with the annotation/computational analyses.

AUTHOR CONTRIBUTIONS

Conceptualization, A.C.M and K.D.S.; Investigation, A.C.M. and S.G.H.; Resources, M.A.; Writing – Original Draft, A.C.M. and K.D.S.; Writing – Review & Editing, A.C.M, S.G.H, M.A. and K.D.S.; Funding Acquisition, A.C.M., M.A. and K.D.S.

DECLARATION OF INTERESTS

K.D.S. is a scientific advisor for Nextbiotics, Inc.

Figures

Figure 1. ICP1 overcomes excision-deficient PLE through loss of accessory helicase *helA*. A, Schematic of the PLE 1 response to ICP1 infection. Left, ICP1 infects PLE (+) *V. cholerae* and expresses PexA, which physically interacts with PLE 1-encoded integrase (Int) to direct PLE circularization and excision. Excised PLE 1 replicates to high copy number, inhibits ICP1 replication, and horizontally transduces to neighboring cells when *V. cholerae* undergoes PLE 1-mediated accelerated lysis. Right, when ICP1 *ΔpexA* infects PLE (+) *V. cholerae*, PLE 1 remains integrated in the host chromosome, and rare mutant phage are able to escape and form a plaque. **B,** Tenfold dilutions of ICP1 spotted on a PLE 1 and PLE (-) *V. cholerae* lawn (grey). Zones of killing are shown in black. **C,** Efficiency of plaquing of wild-type (WT) ICP1^{A} or derivatives with the deletions listed on PLE 1 relative to a PLE (-) *V. cholerae* host. Dashed line indicates limit of detection. **D,** Western blot of endogenously FLAG-tagged HelA during infection of PLE (-) *V. cholerae*. **E,** Quantification of change in ICP1 genome copy number following 20 minutes of infection of the listed *V. cholerae* host as detected by qPCR.

Figure 2. ICP1-encoded *helA* is necessary for PLE replication. A, Quantification of change in PLE 1 copy number following infection by the listed ICP1 strain as measured by qPCR. Empty vector (P_{tac}-*EV*) and *helA* (P_{tac}-*helA*) expression plasmids were induced 20 minutes prior to phage infection. The dashed line indicates no change in copy number. **B,** Quantification of change in midiPLE copy number following infection of midiPLE (+) *V. cholerae ΔlacZ::*P_{tac}-*repA* with the listed expression plasmid by the listed ICP1 as measured by qPCR. Ectopic *repA* and expression plasmids were induced 20 minutes prior to phage infection. **C,** Change in luminescence of P_{orf2}-*nanoluc* reporter with the listed expression plasmid 20 minutes after infection by ICP1^{A} *ΔhelA* relative to the change in luminescence following infection by ICP1^{A}.

Figure 3. Excision and replication deficient PLE is susceptible to ICP1-mediated chromosomal degradation. A, Cartoon of miniPLE during ICP1 infection. Top, miniPLE-

545 encoded Int (circle) is directed to excise miniPLE during ICP1 infection by ICP1-encoded PexA
546 (triangle), leading to a single-copy circularized miniPLE episome. Bottom, catalytically dead
547 miniPLE$_{CD}$ Int (circle with red star) is unable to excise miniPLE during ICP1 infection, potentially
548 rendering the miniPLE susceptible to phage-mediated chromosomal degradation (pac-man). **B,**
549 Circularization PCR of the miniPLE indicated from boiled ICP1^{A} plaques on the host indicated.
550 **C,** (Top) Total DNA prepped from equal numbers of miniPLE or miniPLE$_{CD}$ cells infected by
551 ICP1^{A} at the listed timepoints and imaged via Southern blot (bottom) with a probe against the
552 miniPLE *kanR* cassette. **D,** Change in copy number of the miniPLE indicated 30 minutes
553 following ICP1^{A} infection as measured by qPCR.
554
555 **Figure 4. ICP1 encodes one of two accessory helicase alleles. A,** Plaque size of listed
556 phage on PLE (-) *V. cholerae*. *p<0.01. **B,** Cartoon of ICP1 accessory helicase locus. Grey
557 arrows indicate gene products shared between the two phages, while the mint arrows indicate
558 gene products unique to the *helA* locus and turquoise arrows indicate gene products unique to
559 the *helB* locus. **C,** Map (Vecteezy 2019) of distribution of SF1B-type helicases alleles in ICP1
560 isolates shed by cholera patients in Bangladesh. Top, map of Bangladesh with Dhaka and
561 Mathbaria marked. Bottom, agarose gel showing PCR detection of the conserved DNA
562 polymerase (*gp58)*, *helA*, and *helB* in ICP1 isolates from cholera patient stools collected in
563 Dhaka or Mathbaria. Phage isolates are listed in Table S8.
564
565 **Figure 5. Loss of *helB* permits escape from PLE but leads to a defect in ICP1 fitness. A,**
566 Western blot of endogenously FLAG-tagged *helB* at the listed time points following infection of
567 PLE (-) *V. cholerae*. **B,** Tenfold dilutions of ICP1 spotted on the listed *V. cholerae* lawns. **C,** Fold
568 change in ICP1 copy number following 20 minutes of infection of the listed *V. cholerae* host as
569 measured by qPCR. **D,** Fold change in ICP1 copy number following 20 minutes of infection of
570 the listed *V. cholerae* host as measured by qPCR. Ectopic expression was induced 20 minutes

prior to phage infection. **E,** Plaque size of listed phage on PLE (-) *V. cholerae*. **p<0.001, *ns* not significant.

Figure 6. PLEs can exploit unrelated phage-encoded SF1B-type helicases for replication. Replication of PLE 1 (**A,C**) or midiPLE (**B**) 20 minutes following infection of *V. cholerae* with the listed expression vectors by the listed ICP1^{B} variant as measured by qPCR. Vectors were induced 20 minutes prior to infection. Dashed line indicates no change in copy. **D,** Replication of the listed PLE in an isogenic *V. cholerae* background 20 minutes following infection by ICP1^{A} *ΔhelA*. Ectopic vectors were induced 20 minutes prior to infection. Dashed line indicates no change in copy. **E,** Replication of PLE 1 20 minutes following infection by the listed phage as measured by qPCR. Ectopic expression of *dda* from *E. coli* phage T4 was induced 20 minutes prior to infection. Dashed line indicates no change in copy.

Supplementary Figures

Figure S1. Related to Figure 1. ICP1^{A} *ΔpexA ΔhelA* does not accumulate mutations to escape PLE. Three sets of plaques (a-c) from ICP1 *ΔpexA ΔhelA* on PLE 1 *V. cholerae* were picked and the efficiency of plaquing on PLE 1 relative to PLE (-) *V. cholerae* was tested.

Figure S2. Related to Figure 2. Infected PLE *1 V. cholerae* demonstrate altered lysis kinetics when PLE 1 does not replicate. A, OD_{600} of the PLE 1 *V. cholerae* over time after infection with the listed ICP1. **B,** Cartoon of the PLE 1-encoded nanoluciferase reporter with nanoluciferase (nL) encoded downstream of PLE 1 *orf2.* Line break in the PLE genome is shown for simplicity and no other mutations are present.

Figure S3. Related to Figure 4. SF1B-type helicases are found in a variety of marine phages. A, Praline alignment (Bawono & Heringa 2014) of ICP1^{A} HelA, ICP1^{B} HelB, and T4

Dda. The Walker A motif used in ATP hydrolysis is indicated by asterisks, and the Duf2493 in HelB is underlined. **B,** Phylogenetic analysis of SF1B-type helicases, phages used are listed in Table S7.

Figure S4. Related to Figure 6. PLE replication is not altered by ectopic expression of *helA* or *helB*. Replication of the listed PLE in an isogenic *V. cholerae* background 20 minutes following infection by ICP1^{A}. Ectopic vectors were induced 20 minutes prior to infection. Dashed line indicates no change in copy.

STAR Methods

CONTACT FOR REAGENT AND RESOURCE SHARING

Further information and requests for resources and reagents should be directed to and will be fulfilled by the lead Contact Kimberley Seed (kseed@berkeley.edu).

EXPERIMENTAL MODEL AND SUBJECT DETAILS

Bacterial Growth Conditions

The bacterial strains and plasmids used in this study are listed in Tables S2 and S5. All bacterial strains were grown at 37°C in LB with aeration or on LB agar plates. The following antibiotics were used as necessary: streptomycin (100 μg/mL), spectinomycin (100 μg/mL), kanamycin (75 μg/mL), ampicillin, (*V. cholerae* 50 μg/mL, *E. coli* 100 μg/mL), chloramphenicol (*V. cholerae* 1.25 μg/mL, *E. coli* 25 μg/mL). Ectopic expression constructs in *V. cholerae* were induced 20 minutes prior to ICP1 infection with 1 mM Isopropyl β-D-1-thiogalactopyranoside (IPTG) and 1.5 mM theophylline.

621 **Phage Growth Conditions**

622 The phage isolates used in this study are listed in Table S3. Phage were propagated using the
623 soft agar overly method and high titer stocks were made by polyethylene glycerol precipitation
624 and stored in sodium chloride-tris-EDTA (STE) buffer (Clokie & Kropinski 2009).

625

626 **Phage isolation from rice water stool**

627 The collection of cholera patient rice water stool (RWS) was approved by the icddr,b
628 institutional review board. All samples were deidentified and written informed consent was
629 obtained from adult participants and from the guardians of children. Stool samples were mixed
630 with glycerol in cryovials, frozen, until being processed at the University of California, Berkeley.
631 For processing, samples were thawed and grown on thiosulfate-citrate-bile salts-sucrose agar,
632 or used to inoculate alkaline peptone water (APW) for outgrowth. Liquid APW cultures were
633 struck out on agar plates and aliquots were frozen with glycerol. Individual colonies selected
634 from plates were confirmed as *V. cholerae* by PCR. These isolates of *V. cholerae*, in addition to
635 the PLE (-) laboratory strain, were used to isolate phages directly from the RWS glycerol stocks
636 and from frozen APW outgrowths. Isolated phages were plaque purified twice after isolation.

637

638 **METHOD DETAILS**

639 **Bacterial and phage cloning conditions**

640 Bacterial mutants were cloned using SOE (splicing by overlap extension) PCR and introduced
641 by natural transformation (Dalia et al. 2014). Plasmids were constructed using Gibson Assembly
642 or Golden Gate Assembly. Phage mutants were constructed using CRISPR-Cas engineering as
643 previously described (Box et al. 2016; McKitterick & Seed 2018). Briefly, an editing template
644 with the desired deletion was cloned into a plasmid and *V. cholerae* harboring this plasmid was
645 infected by the ICP1 strain of interest. Ten plaques of the passaged phage were collected and
646 mutants were selected on *V. cholerae* engineered to encode an inducible Type 1-E CRISPR-

Cas system and a plasmid with a spacer targeting the gene of interest. Mutant phages were verified via Sanger sequencing and purified two times on the targeting host before storing in STE. Total phage gDNA was prepped with a DNeasy Blood & Tissue Kit (Qiagen).

Phage plaquing conditions

Spot plates were performed as before (McKitterick & Seed 2018). Briefly, mid-log *V. cholerae* was added to 0.5% molten LB agar poured on a solid agar plate and allowed to solidify. Ten-fold dilutions of phage were applied to the surface in 3 μL spots and allowed to dry. Plates were incubated at 37°C. Images are representative of at least two independent experiments. The efficiency of plaquing (EOP) was calculated by comparing the number of plaques a given phage forms on PLE (-) *V. cholerae* relative to the number of plaques formed on PLE (+) *V. cholerae*. Each EOP was calculated in triplicate, and the limit of detection is the point at which the phage is unable to productively infect the PLE (+) host while still forming plaques on a PLE (-) host. Plaque size was determined by imaging and quantifying with ImageJ at least 20 plaques each from 3 independent replicates in 0.5% agar overlay on PLE (-) *V. cholerae*. Significance was determined through a nonparametric T Test.

qPCR conditions

Fold change in genome copy was performed as before (O'Hara et al. 2017) with slight modification. Fold change in ICP1 copy number was measured by growing cells to an OD_{600} of 0.3, infected with a multiplicity of infection (MOI) of 0.01, and a sample was boiled for 10 minutes as a starting value. Infected cells were returned to the incubator for 20 minutes, at which point another sample was taken and boiled. Boiled samples were diluted 1:50 and used as a template in the qPCR reaction. To measure the fold change in PLE and midiPLE copy number, cells were grown to an OD_{600} = 0.3 and the initial sample was immediately taken prior to addition of phage at an MOI of 2.5 and boiled for 10 minutes. Samples were taken at 20

minutes after infection, boiled for 10 minutes, and diluted 1:1000. Quantification of the fold change in miniPLE copy was measured during infection with an MOI of 5, with samples taken immediately prior to infection and 30 minutes after infection and boiled for 10 minutes. Boiled samples were diluted 1:100 and used as template. Experiments with ectopic expression constructs were induced at OD_{600} = 0.2 for 20 minutes and then normalized to OD_{600} = 0.3 prior to infection. All samples were run in biological triplicates and technical duplicates. The template was mixed with the primers listed in Table S4 and IQ Sybr Green Master Mix (Bio-rad) and run on a CFX Connect Real-Time PCR Detection System (Bio-rad). Fold change was measured as the amount of DNA in the sample at 20 or 30 minutes after infection relative to the amount of DNA in the sample at T=0. Significance was measured by 2-tailed T Test.

Western Blots

PLE (-) *V. cholerae* was grown to an OD_{600} = 0.3 and infected with the endogenously FLAG-tagged ICP1 listed. At the listed timepoints, 1 mL samples were collected and mixed with equal volume ice-cold methanol and centrifuged at 13000 rpm for 3 minutes at 4°C. Pellets were washed with ice-cold PBS, resuspended in 1x Laemmli buffer, and boiled for 10 minutes at 99°C. Total protein was run on a 10% Stain Free TGX SDS-PAGE gel (Bio-rad). Primary Rabbit-α-FLAG antibodies (Sigma) were used at a dilution of 1:5000 and detected with goat-α-rabbit-HRP conjugated secondary antibodies at a dilution of 1:5000 (Bio-rad). Clarity Western ECL Substrate (Bio-rad) was used to develop the blots and a Chemidoc XRS Imaging System (Bio-rad) was used to image.

Lysis kinetics and Nanoluciferase assay

PLE (+) *V. cholerae* cells were grown to an OD_{600} = 0.2 and the listed ectopic expression constructs were induced for 20 minutes. Cells were then normalized to an OD_{600} = 0.3 and infected at an MOI of 2.5. For lysis kinetics, OD_{600} was monitored for 30 minutes. For

699 nanoluciferase, 100 µL cells were sampled at T=0 and T=20 minutes after infection and added
700 to 100 µL ice cold methanol. Luminescence was measured in a Spectra Max i3x plate reader
701 (Molecular Devices) using the Nano-Glo Luciferase Assay System (Promega). Relative
702 luminescence was calculated by dividing the luminescence detected after infection with the
703 knockout phage relative to the luminescence detected after infection with the WT phage.
704
705 **PCR conditions**
706 PLE circularization PCRs were performed as described (McKitterick & Seed 2018). Briefly,
707 plaques on the miniPLE or miniPLE$_{CD}$ hosts were picked into 50 µL of water and boiled for 10
708 minutes. Boiled template (2 µL) was used with the primers listed in Table S4 to detect miniPLE
709 circularization. Detection of ICP1 *DNA pol, helA,* and *helB* from ICP1 isolates were performed
710 on 5 – 30 ng prepped gDNA from isolated phage with the primers listed in Table S4. PCRs were
711 run on 2% agarose gels and visualized with GelGreen.
712
713 **Southern Blots**
714 A probe against miniPLE was created using the DIG-High Prime DNA Labeling and Detection
715 Started Kit I (Sigma). Cells were grown up to OD_{600} = 0.3 with kanamycin and infected with
716 ICP1^{A} at an MOI of 5. At the timepoints indicated, 5 mL of cells were harvested and mixed with
717 5 mL ice cold methanol. Samples were spun at 7000xg at 4^{o}C for 5 minutes. Pellets were
718 washed ice cold PBS and spun again. Total DNA was extracted from the pellets with the
719 DNeasy Blood & Tissue Kit (Qiagen). Equal volumes of samples (between 1.5 and 4.1 µg DNA)
720 were digested overnight with EcoRV-HF and SalI-HF (NEB) and run on a 0.7% agarose gel and
721 visualized with GelRed. The agarose gel was washed briefly and incubated with 0.25 N HCl for
722 15 minutes, washed again, denatured in 0.4 M NaOH for 20 minutes, and transferred overnight.
723 DNA was fixed by baking the blot at 120 ^{o}C for 30 minutes, and hybridized with 17 ng/mL

724 miniPLE probe overnight at 42°C. The blot was detected with the DIG-High Prime DNA Labeling
725 and Detection Started Kit I (Sigma) and CSPD™ Substrate (ThermoScientific) and visualized on
726 a Chemidoc XRS Imaging System (Bio-rad).
727
728 **Computational analyses**
729 Escape ICP1 *ΔpexA* phage were isolated from PLE (+) *V. cholerae* and purified twice on the
730 same host. Total gDNA was prepped as above. NEBNext Ultra II DNA Library Preparation Kit
731 for Illuminia (New England Biolabs) was used to prep genomic DNA and was sequenced by
732 paired-end sequencing (2 × 150 bp) on an Illumina HiSeq4000 (University of California,
733 Berkeley QB3 Core Facility). The wild-type phage genome was assembled using SPAdes
734 (Bankevich et al. 2012) with paired-end reads and default settings. This assembly was used as
735 the reference sequence for comparison to escape phage sequence reads with breseq
736 (Deatherage & Barrick 2014) in 'consensus' mode and default settings. Protein alignments were
737 analyzed using Praline (Bawono & Heringa 2014). HelA conservation was determined by
738 analyzing HelA from 17 phages isolated between 2001 and 2017 (Angermeyer et al. 2018;
739 McKitterick et al. 2019). Phages that did not have whole genome information were Sanger
740 sequenced from previously prepped phage gDNA (McKitterick et al. 2019) with the primers
741 listed in Table S4. Phages included in the phylogenetic analysis were selected from a BLASTP
742 search of HelA and HelB. Each hit was included if it had over 30% identity to either protein
743 across 90% of the protein. A multiple alignment of helicase amino acid sequences was
744 generated with MUSCLE v3.8.31 (Edgar 2004) using default settings. The alignment file was
745 converted to the PHYLIP format with Clustal X v2.0 (Larkin et al. 2007) and a bootstrapped
746 (n=100) maximum-likelihood phylogenetic tree was solved using PhyML v20120412 (Guindon et
747 al. 2005) with the following settings: -d aa -s BEST --rand_start --n_rand_starts 100 -o tlr -b
748 100).
749

Quantification and statistical analysis

Statistical tests used for experiments are listed in the Methods section. Data was analyzed using Prism GraphPad. For EOPs, qPCR, lysis kinetics, and nanoluciferase assays, error bars indicate standard deviation of average fold change from three independent biological replicates. Spot plate, agarose gel, and blot images are representative of at least two independent experiments.

Data and code availability

The data supporting the study are found in the manuscript, supplementary information, or from the corresponding author upon request.

References

Angermeyer, A. et al., 2018. Analysis of 19 Highly Conserved *Vibrio cholerae* Bacteriophages Isolated from Environmental and Patient Sources Over a Twelve-Year Period. *Viruses*, 10(6), p.299.

Bankevich, A. et al., 2012. SPAdes: A New Genome Assembly Algorithm and Its Applications to Single-Cell Sequencing. *Journal of Computational Biology*, 19(5), pp.455–477.

Barth, Z.K. et al., 2019. Genome replication dynamics of a bacteriophage and its satellite reveal strategies for parasitism and viral restriction. *bioRxiv*. Available at: https://www.biorxiv.org/content/10.1101/639039v1.

Bawono, P. & Heringa, J., 2014. PRALINE: A Versatile Multiple Sequence Alignment Toolkit. *Methods Mol Bio*, 1079, pp.245–62.

Blair, L.P., Tackett, A.J. & Raney, K.D., 2009. Development and evaluation of a structural model for SF1B helicase dda. *Biochemistry*, 48(11), pp.2321–2329.

Bondy-Denomy, J. & Davidson, A.R., 2014. When a virus is not a parasite: The beneficial effects of prophages on bacterial fitness. *Journal of Microbiology*, 52(3), pp.235–242.

Bowring, J. et al., 2017. Pirating conserved phage mechanisms promotes promiscuous staphylococcal pathogenicity island transfer. *eLife*, 6, p.e26487.

Box, A.M. et al., 2016. Functional analysis of bacteriophage immunity through a Type I-E CRISPR-Cas system in *Vibrio cholerae* and its application in bacteriophage genome engineering. *Journal of Bacteriology*, 198(3), pp.578–90.

Brister, J.R., 2008. Origin Activation Requires both Replicative and Accessory Helicases during T4 Infection. *Journal of Molecular Biology*, 377(5), pp.1304–1313.

Brüssow, H., Canchaya, C. & Hardt, W.-D., 2004. Phages and the Evolution of Bacterial Pathogens: from Genomic Rearrangements to Lysogenic Conversion. *Microbiol Mol Biol Rev*, 68(3), pp.560–602.

Byrd, A.K. & Raney, K.D., 2006. Displacement of a DNA binding protein by Dda helicase.

Nucleic Acids Research, 34(10), pp.3020–3029.

Byrd, A.K. & Raney, K.D., 2017. Structure and function of Pif1 helicase. *Biochemical Society Transactions*, 45(5), pp.1159–1171.

Chen, J. et al., 2018. Genome hypermobility by lateral transduction. *Science*, 362(6411), pp.207–212.

Clokie, M.R.J. & Kropinski, A.M. eds., 2009. *Bacteriophages : methods and protocols*, Humanan Press.

Crow, M.S. et al., 2016. Diverse mechanisms evolved by DNA viruses to inhibit early host defenses. *Critical Reviews in Biochemistry and Molecular Biology*, 51(6), pp.452–481.

Dalia, A.B., Lazinski, D.W. & Camilli, A., 2014. Identification of a Membrane-Bound Transcriptional Regulator That Links Chitin and Natural Competence in *Vibrio cholerae*. *mBio*, 5(1), pp.e01028-13.

Deatherage, D.E. & Barrick, J., 2014. *Evolved Microbes from Next-Generation Sequencing Data Using breseq, in Engineering and Analyzing Multicellular Systems: Methods and Protocols* L. Sun & W. Shou, eds., New York, New York: Springer.

Doron, S. et al., 2018. Systematic discovery of antiphage defense systems in the microbial pangenome. *Science*, 359(6379), p.eaar4120.

Dy, R.L. et al., 2014. Remarkable Mechanisms in Microbes to Resist Phage Infections. *Annual Review of Virology*, 1(1), pp.307–331.

Edgar, R.C., 2004. MUSCLE : multiple sequence alignment with high accuracy and high throughput. *Nucleic Acids Res*, 32(5), pp.1792–1797.

Faruque, S.M. et al., 2005. Self-limiting nature of seasonal cholera epidemics: Role of host-mediated amplification of phage. *Proceedings of the National Academy of Sciences*, 102(17), pp.6119–6124.

Fillol-Salom, A. et al., 2018. Phage-inducible chromosomal islands are ubiquitous within the bacterial universe. *ISME Journal*, 12(9), pp.2114–2128.

Guindon, S. et al., 2005. PHYML Online — a web server for fast maximum likelihood-based phylogenetic inference. *Nucleic Acids Research*, 33(Web Server issue), pp.W557–W559.

He, X. et al., 2012. The T4 phage SF1B helicase Dda is structurally optimized to perform DNA strand separation. *Structure*, 20(7), pp.1189–1200.

Hercules, K. et al., 1971. Mutants in a Nonessential Gene of Bacteriophage T4 Which Are Defective in the Degradation of Escherichia coli Deoxyribonucleic Acid. *J Virol*, 7(I), pp.95–105.

Hille, F. et al., 2018. The Biology of CRISPR-Cas: Backward and Forward. *Cell*, 172(6), pp.1239–1259.

Hinton, D.M. et al., 2005. Transcriptional takeover by σ appropriation: Remodelling of the σ70 subunit of Escherichia coli RNA polymerase by the bacteriophage T4 activator MotA and co-activator AsiA. *Microbiology*, 151(6), pp.1729–1740.

Kauffman, K.M. et al., 2018. Viruses of the Nahant Collection, characterization of 251 marine Vibrionaceae viruses. *Scientific Data*, 5, p.180114.

Keen, E.C. et al., 2017. Novel “Superspreader” Bacteriophages Promote Horizontal Gene Transfer by Transformation. *mBio*, 8(1), pp.e02115-16.

Koonin, E. V & Krupovic, M., 2015. Evolution of adaptive immunity from transposable elements combined with innate immune systems. *Nat Rev Genet*, 16(3), pp.184–192.

Koskella, B. & Brockhurst, M.A., 2014. Bacteria-phage coevolution as a driver of ecological and evolutionary processes in microbial communities. *FEMS Microbiology Reviews*, 38(5), pp.916–931.

Larkin, M.A. et al., 2007. Clustal W and Clustal X version 2.0. *Bioinformatics*, 23(21), pp.2947–2948.

Makarova, K.S. et al., 2011. Defense Islands in Bacterial and Archaeal Genomes and Prediction of Novel Defense Systems. *Journal of Bacteriology*, 193(21), pp.6039–6056.

Manrique, P., Dills, M. & Young, M.J., 2017. The Human Gut Phage Community and Its

839 Implications for Health and Disease. *Viruses*, 9(6), p.E141.

840 Martínez-Rubio, R. et al., 2017. Phage-inducible islands in the Gram-positive cocci. *The ISME*
841 *Journal*, 11(4), pp.1029–1042.

842 McKitterick, A.C. et al., 2019. Competition between mobile genetic elements drives optimization
843 of a phage-encoded CRISPR-Cas system: Insights from a natural arms-race. *Phil. Trans.*
844 *R. Soc. B*, 374(1772), p.20180089.

845 McKitterick, A.C. & Seed, K.D., 2018. Anti-phage islands force their target phage to directly
846 mediate island excision and spread. *Nature Communications*, 9(1), p.2348.

847 O'Hara, B.J. et al., 2017. A highly specific phage defense system is a conserved feature of the
848 *Vibrio cholerae* mobilome. *PLoS Genetics*, 13(6), p.e1006838.

849 Penadés, J.R. et al., 2015. Bacteriophage-mediated spread of bacterial virulence genes.
850 *Current Opinion in Microbiology*, 23, pp.171–8.

851 Penadés, J.R. & Christie, G.E., 2015. The Phage-Inducible Chromosomal Islands: A Family of
852 Highly Evolved Molecular Parasites. *Annual Review of Virology*, 2(1), pp.181–201.

853 Pires, D.P. et al., 2016. Genetically Engineered Phages: a Review of Advances over the Last
854 Decade. *Microbiology and Molecular Biology Reviews*, 80(3), pp.523–543.

855 Ram, G. et al., 2012. Staphylococcal pathogenicity island interference with helper phage
856 reproduction is a paradigm of molecular parasitism. *Proceedings of the National Academy*
857 *of Sciences*, 109(40), pp.16300–16305.

858 Rivas, H.G., Schmaling, S.K. & Gaglia, M.M., 2016. Shutoff of host gene expression in influenza
859 A virus and herpesviruses: Similar mechanisms and common themes. *Viruses*, 8(4), p.102.

860 Saikrishnan, K. et al., 2009. Mechanistic Basis of 5′-3′ Translocation in SF1B Helicases. *Cell*,
861 137(5), pp.849–859.

862 Samson, J.E. et al., 2013. Revenge of the phages: defeating bacterial defences. *Nat Rev*
863 *Microbiol*, 11(10), pp.675–87.

864 Seed, K.D. et al., 2013. A bacteriophage encodes its own CRISPR/Cas adaptive response to

865 evade host innate immunity. *Nature*, 494(7438), pp.489–91.

866 Seed, K.D. et al., 2011. Evidence of a Dominant Lineage of *Vibrio cholerae*-Specific Lytic
867 Bacteriophages Shed by Cholera Patients over a 10-Year Period in Dhaka, Bangladesh.
868 *mBio*, 2(1), pp.e00334-10.

869 Seed, K.D. et al., 2014. Evolutionary consequences of intra-patient phage predation on
870 microbial populations. *eLife*, 3, p.e03497.

871 Singleton, M.R. et al., 2004. Crystal structure of RecBCD enzyme reveals a machine for
872 processing DNA breaks. *Nature*, 432(7014), pp.187–193.

873 Tormo-Más, M.A. et al., 2010. Moonlighting bacteriophage proteins derepress staphylococcal
874 pathogenicity islands. *Nature*, 465(7299), pp.779–782.

875 Ubeda, C. et al., 2009. Specificity of staphylococcal phage and SaPI DNA packaging as
876 revealed by integrase and terminase mutations. *Mol Microbiol.*, 72(1), pp.98–108.

877 Úbeda, C. et al., 2008. SaPI mutations affecting replication and transfer and enabling
878 autonomous replication in the absence of helper phage. *Molecular Microbiology*, 67(3),
879 pp.493–503.

880 Vecteezy, 2019. Vector Bangladesh Map. Available at: https://www.vecteezy.com/.

881 Warner, H.R. et al., 1970. Isolation of Bacteriophage T4 Mutants Defective in the Ability to
882 Degrade Host Deoxyribonucleic Acid. *J Virol*, 5(6), pp.700–708.

883

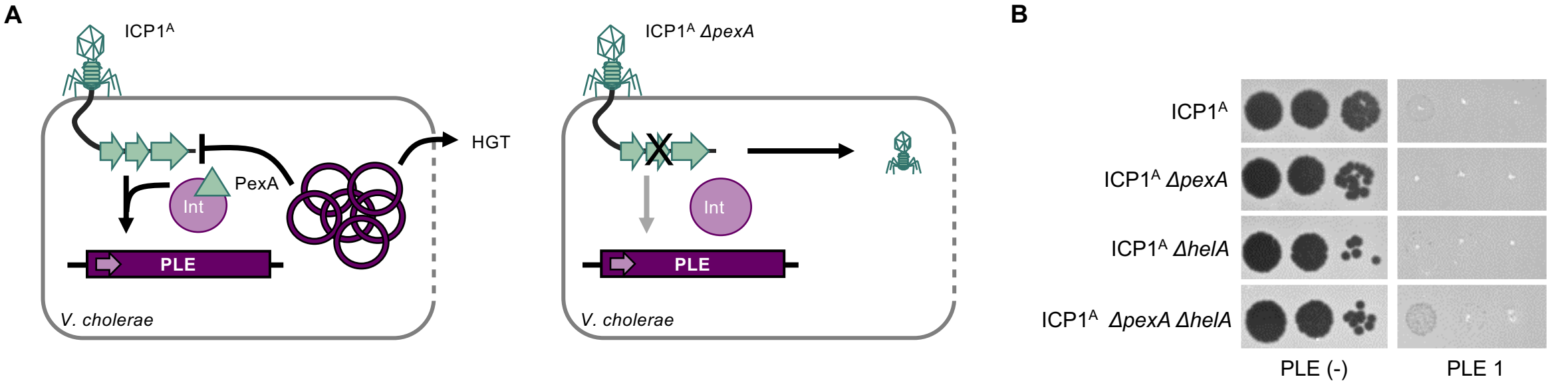

Figure 1. ICP1 overcomes excision-deficient PLE through loss of accessory helicase *helA*. A, Schematic of the PLE 1 response to ICP1 infection. Left, ICP1 infects PLE (+) *V. cholerae* and expresses PexA, which physically interacts with PLE 1-encoded integrase (Int) to direct PLE circularization and excision. Excised PLE 1 replicates to high copy number, inhibits ICP1 replication, and horizontally transduces to neighboring cells when *V. cholerae* undergoes PLE 1-mediated accelerated lysis. Right, when ICP1 *ΔpexA* infects PLE (+) *V. cholerae*, PLE 1 remains integrated in the host chromosome, and rare mutant phage are able to escape and form a plaque. **B,** Tenfold dilutions of ICP1 spotted on a PLE 1 and PLE (-) *V. cholerae* lawn (grey). Zones of killing are shown in black. **C,** Efficiency of plaquing of wild-type (WT) ICP1^{A} or derivatives with the deletions listed on PLE 1 relative to a PLE (-) *V. cholerae* host. Dashed line indicates limit of detection. **D,** Western blot of endogenously FLAG-tagged HelA during infection of PLE (-) *V. cholerae*. **E,** Quantification of change in ICP1 genome copy number following 20 minutes of infection of the listed *V. cholerae* host as detected by qPCR.

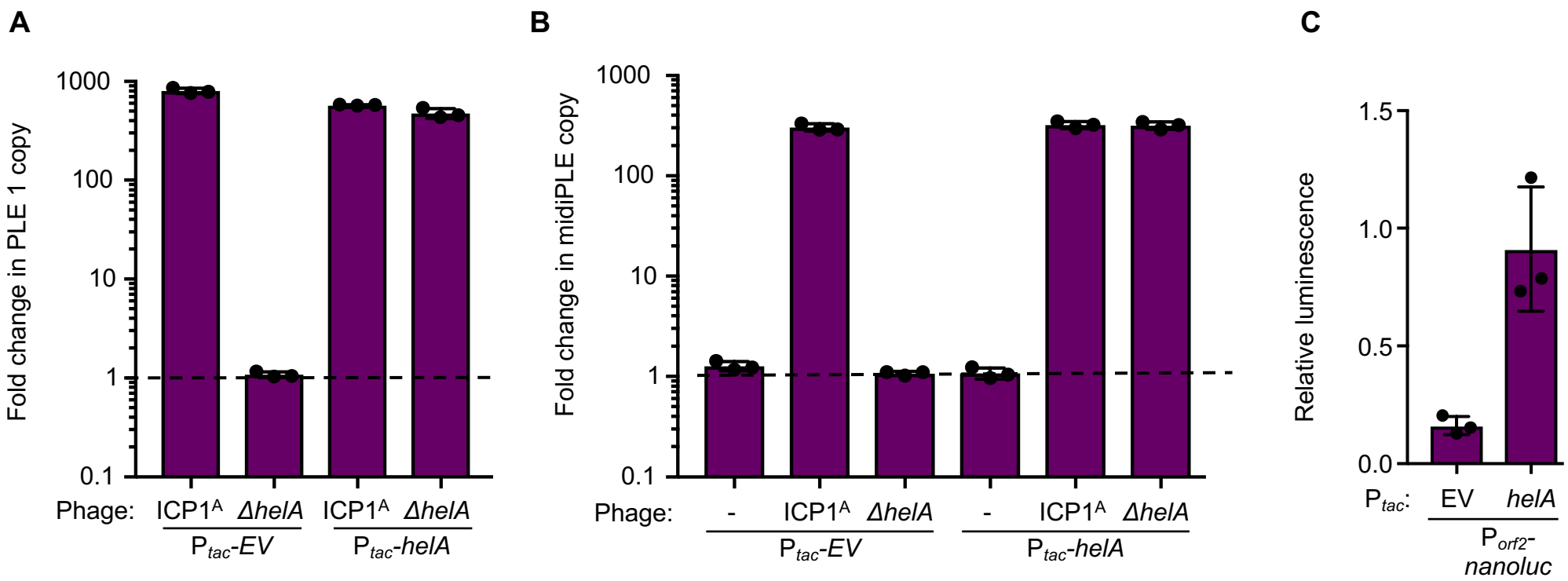

Figure 2. ICP1-encoded *helA* is necessary for PLE replication. A, Quantification of change in PLE 1 copy number following infection by the listed ICP1 strain as measured by qPCR. Empty vector (P_{tac}-*EV*) and *helA* (P_{tac}-*helA*) expression plasmids were induced 20 minutes prior to phage infection. The dashed line indicates no change in copy number. **B,** Quantification of change in midiPLE copy number following infection of midiPLE (+) *V. cholerae ΔlacZ::*P_{tac}-*repA* with the listed expression plasmid by the listed ICP1 as measured by qPCR. Ectopic *repA* and expression plasmids were induced 20 minutes prior to phage infection. **C,** Change in luminescence of P_{orf2}-*nanoluc* reporter with the listed expression plasmid 20 minutes after infection by ICP1^A *ΔhelA* relative to the change in luminescence following infection by ICP1^A.

Figure 3. Excision and replication deficient PLE is susceptible to ICP1-mediated chromosomal degradation. A, Cartoon of miniPLE during ICP1 infection. Top, miniPLE-encoded Int (circle) is directed to excise miniPLE during ICP1 infection by ICP1-encoded PexA (triangle), leading to a single-copy circularized miniPLE episome. Bottom, catalytically dead miniPLE$_{CD}$ Int (circle with red star) is unable to excise miniPLE during ICP1 infection, potentially rendering the miniPLE susceptible to phage-mediated chromosomal degradation (pac-man). **B,** Circularization PCR of the miniPLE indicated from boiled ICP1^{A} plaques on the host indicated. **C,** (Top) Total DNA prepped from equal numbers of miniPLE or miniPLE$_{CD}$ cells infected by ICP1^{A} at the listed timepoints and imaged via Southern blot (bottom) with a probe against the miniPLE *kanR* cassette. **D,** Change in copy number of the miniPLE indicated 30 minutes following ICP1^{A} infection as measured by qPCR.

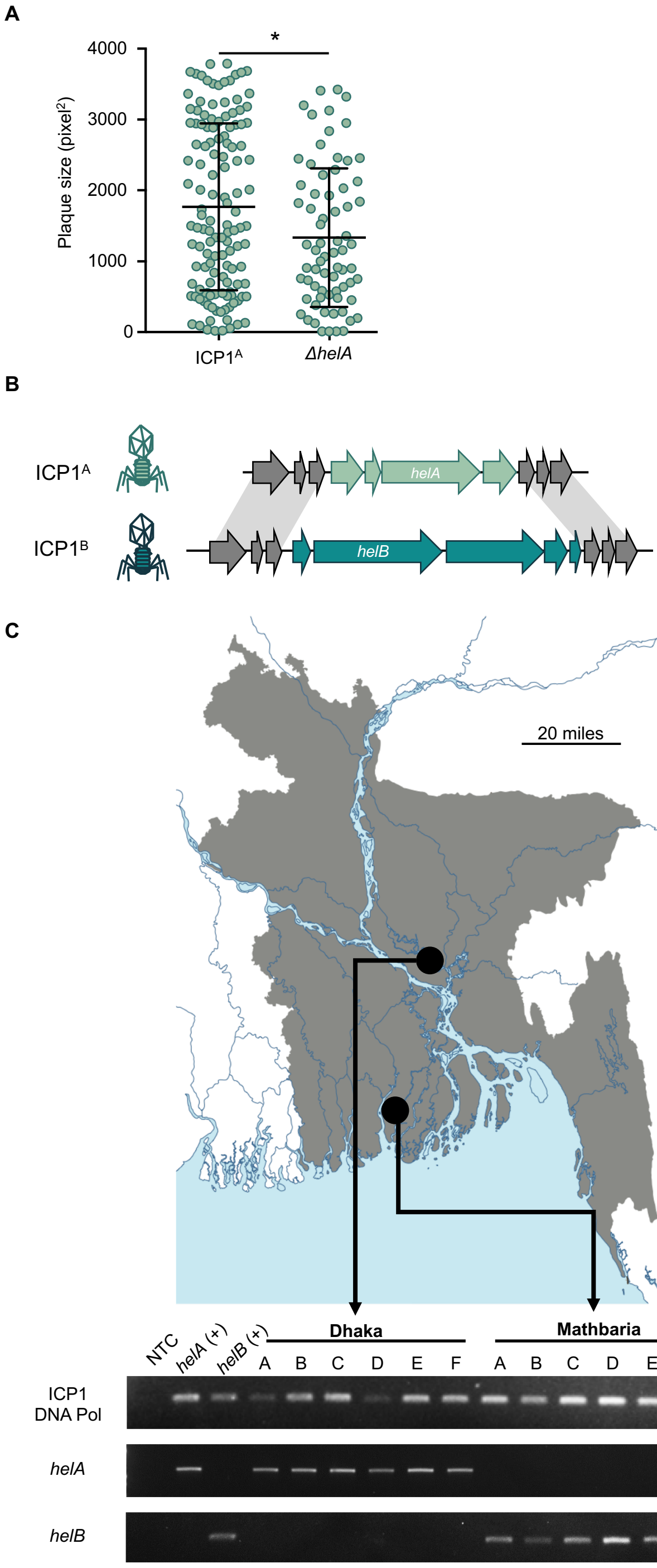

Figure 4. ICP1 encodes one of two accessory helicase alleles. A, Plaque size of listed phage on PLE (-) *V. cholerae*. *p<0.01. **B,** Cartoon of ICP1 accessory helicase locus. Grey arrows indicate gene products shared between the two phages, while the mint arrows indicate gene products unique to the *helA* locus and turquoise arrows indicate gene products unique to the *helB* locus. **C,** Map (Vecteezy 2019) of distribution of SF1B-type helicases alleles in ICP1 isolates shed by cholera patients in Bangladesh. Top, map of Bangladesh with Dhaka and Mathbaria marked. Bottom, agarose gel showing PCR detection of the conserved DNA polymerase (*gp58)*, *helA*, and *helB* in ICP1 isolates from cholera patient stools collected in Dhaka or Mathbaria. Phage isolates are listed in Table S8.

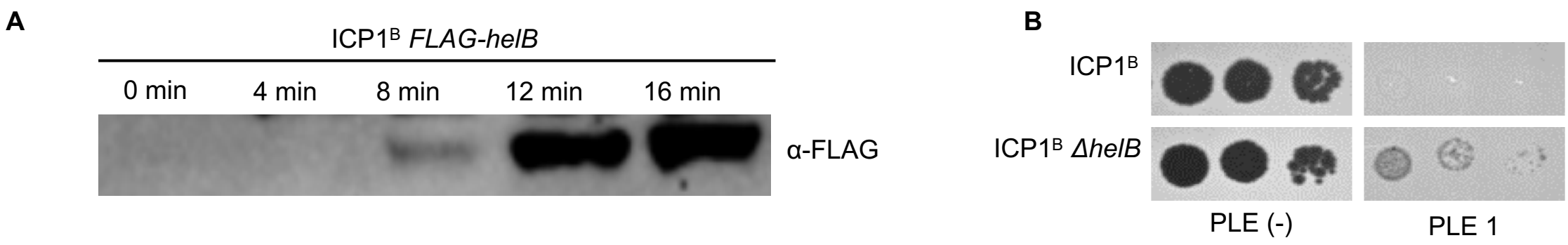

Figure 5. Loss of *helB* permits escape from PLE but leads to a defect in ICP1 fitness. A, Western blot of endogenously FLAG-tagged *helB* at the listed time points following infection of PLE (-) *V. cholerae*. **B,** Tenfold dilutions of ICP1 spotted on the listed *V. cholerae* lawns. **C,** Fold change in ICP1 copy number following 20 minutes of infection of the listed *V. cholerae* host as measured by qPCR. **D,** Fold change in ICP1 copy number following 20 minutes of infection of the listed *V. cholerae* host as measured by qPCR. Ectopic expression was induced 20 minutes prior to phage infection. **E,** Plaque size of listed phage on PLE (-) *V. cholerae*. **p<0.001, *ns* not significant.

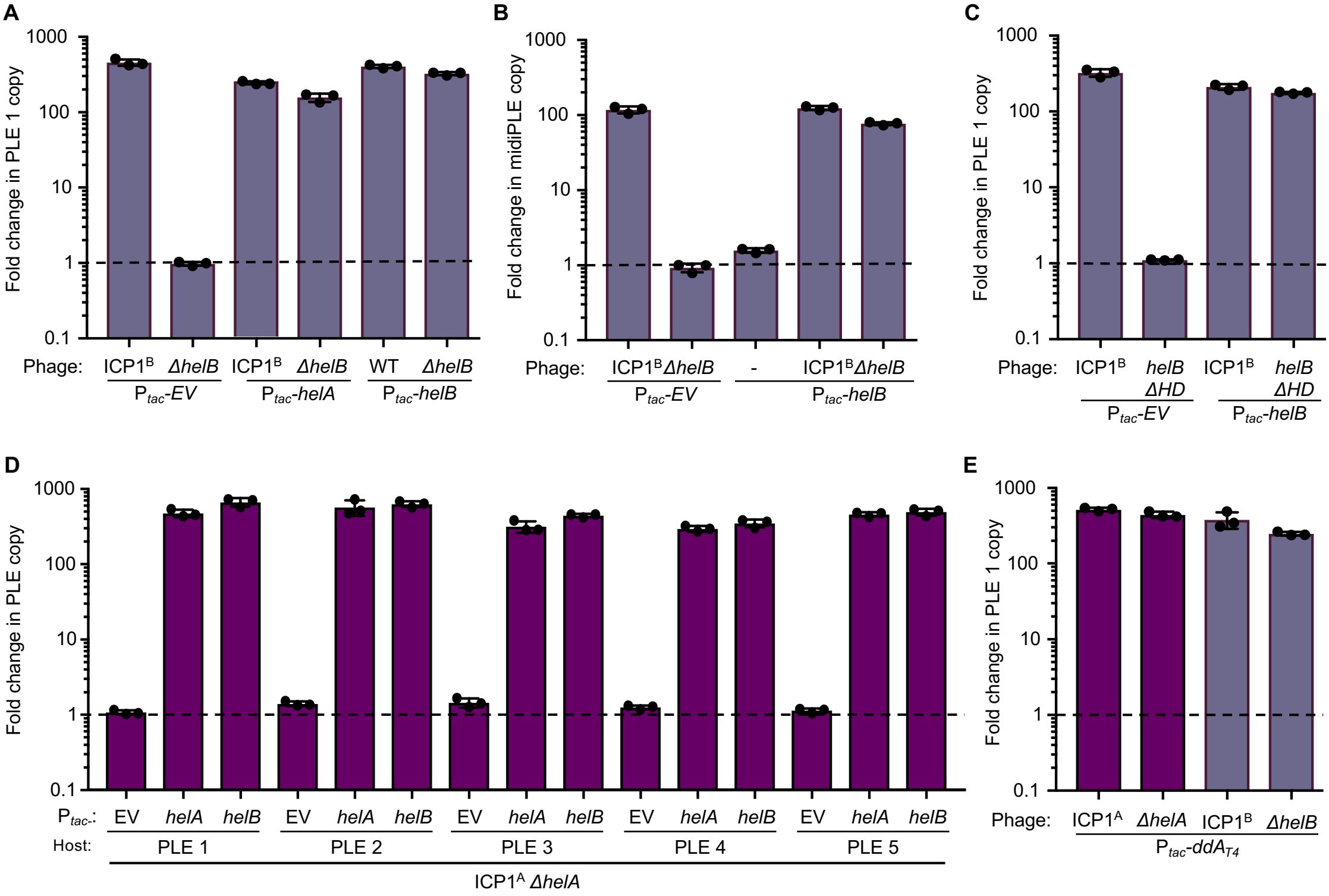

Figure 6. PLEs can exploit unrelated phage-encoded SF1B-type helicases for replication. Replication of PLE 1 (**A,C**) or midiPLE (**B**) 20 minutes following infection of *V. cholerae* with the listed expression vectors by the listed ICP1^{B} variant as measured by qPCR. Vectors were induced 20 minutes prior to infection. Dashed line indicates no change in copy. **D,** Replication of the listed PLE in an isogenic *V. cholerae* background 20 minutes following infection by ICP1^{A} *ΔhelA*. Ectopic vectors were induced 20 minutes prior to infection. Dashed line indicates no change in copy. **E,** Replication of PLE 1 20 minutes following infection by the listed phage as measured by qPCR. Ectopic expression of *dda* from *E. coli* phage T4 was induced 20 minutes prior to infection. Dashed line indicates no change in copy.